THE *CHANDRA* PLANETARY NEBULA SURVEY (ChanPlaNS). II.
X-RAY EMISSION FROM COMPACT PLANETARY NEBULAE

M. Freeman[1], R. Montez Jr.[2], J. H. Kastner[1], B. Balick[3], D. J. Frew[4], D. Jones[5,6], B. Miszalski[7,8],
R. Sahai[9], E. Blackman[10], Y.-H. Chu[11], O. De Marco[4], A. Frank[10], M. A. Guerrero[12], J. A. Lopez[13], A. Zijlstra[14],
V. Bujarrabal[15], R. L. M. Corradi[16,17], J. Nordhaus[17], Q. A. Parker[4,18], C. Sandin[19], D. Schönberner[19],
N. Soker[20], J. L. Sokoloski[21], M. Steffen[19], J. A. Toalá[12], T. Ueta[22], and E. Villaver[23]

[1] Center for Imaging Science and Laboratory for Multiwavelength Astrophysics, Rochester Institute of Technology,
54 Lomb Memorial Drive, Rochester, NY 14623, USA
[2] Department of Physics & Astronomy, Vanderbilt University, Nashville, TN, USA
[3] Department of Astronomy, University of Washington, Seattle, WA, USA
[4] Department of Physics & Astronomy and Macquarie Research Centre for Astronomy, Astrophysics & Astrophotonics,
Macquarie University, Sydney, NSW 2109, Australia
[5] Departamento de Física, Universidad de Atacama, Copayapu 485, Copiapó, Chile
[6] European Southern Observatory, Alonso de Córdova 3107, Casilla 19001, Santiago, Chile
[7] South African Astronomical Observatory, P.O. Box 9, Observatory, 7935, South Africa
[8] Southern African Large Telescope Foundation, P.O. Box 9, Observatory, 7935, South Africa
[9] Jet Propulsion Laboratory, MS 183-900, California Institute of Technology, Pasadena, CA 91109, USA
[10] Department of Physics & Astronomy, University of Rochester, Rochester, NY, USA
[11] Department of Astronomy, University of Illinois at Urbana-Champaign, Urbana, IL, USA
[12] Instituto de Astrofísica de Andalucía, IAA-CSIC, Glorieta de la Astronomía s/n, Granada, E-18008, Spain
[13] Instituto de Astronomía, Universidad Nacional Autonoma de Mexico, Campus Ensenada, Apdo. Postal 22860, Ensenada, B. C., Mexico
[14] School of Physics and Astronomy, University of Manchester, Manchester M13 9PL, UK
[15] Instituto de Astrofísica de Canarias, E-38200 La Laguna, Tenerife, Spain
[16] Departamento de Astrofísica, Universidad de La Laguna, E-38206 La Laguna, Tenerife, Spain
[17] NSF Astronomy and Astrophysics Fellow, Center for Computational Relativity and Gravitation,
Rochester Institute of Technology, Rochester, NY 14623, USA
[18] Australian Astronomical Observatory, P.O. Box 296, Epping, NSW 2121, Australia
[19] Leibniz Institute for Astrophysics Potsdam (AIP), An der Sternwarte 16, D-14482 Potsdam, Germany
[20] Observatorio Astronomico Nacional, Apartado 112, E-28803, Alcala de Henares, Spain
[21] Columbia Astrophysics Laboratory, Columbia University, New York, NY 10027, USA
[22] Department of Physics & Astronomy, University of Denver, Denver, CO 80208, USA
[23] Departamento de Física Teórica, Universidad Autónoma de Madrid, Cantoblanco, E-28049 Madrid, Spain

ABSTRACT

We present results from the most recent set of observations obtained as part of the *Chandra* X-ray observatory Planetary Nebula Survey (ChanPlaNS), the first comprehensive X-ray survey of planetary nebulae (PNe) in the solar neighborhood (i.e., within ∼1.5 kpc of the Sun). The survey is designed to place constraints on the frequency of appearance and range of X-ray spectral characteristics of X-ray-emitting PN central stars and the evolutionary timescales of wind-shock-heated bubbles within PNe. ChanPlaNS began with a combined Cycle 12 and archive *Chandra* survey of 35 PNe. ChanPlaNS continued via a *Chandra* Cycle 14 Large Program which targeted all (24) remaining known compact ($R_{neb} \lesssim 0.4$ pc), young PNe that lie within ∼1.5 kpc. Results from these Cycle 14 observations include first-time X-ray detections of hot bubbles within NGC 1501, 3918, 6153, and 6369, and point sources in HbDs 1, NGC 6337, and Sp 1. The addition of the Cycle 14 results brings the overall ChanPlaNS diffuse X-ray detection rate to ∼27% and the point source detection rate to ∼36%. It has become clearer that diffuse X-ray emission is associated with young ($\lesssim 5 \times 10^3$ yr), and likewise compact ($R_{neb} \lesssim 0.15$ pc), PNe with closed structures and high central electron densities ($n_e \gtrsim 1000$ cm^{-3}), and is rarely associated with PNe that show H$_2$ emission and/or pronounced butterfly structures. Hb 5 is one such exception of a PN with a butterfly structure that hosts diffuse X-ray emission. Additionally, two of the five new diffuse X-ray detections (NGC 1501 and NGC 6369) host [WR]-type central stars, supporting the hypothesis that PNe with central stars of [WR]-type are likely to display diffuse X-ray emission.

Key words: binaries: general – planetary nebulae: individual (NGC 1501, NGC 3918, NGC 6153, NGC 6369, HbDs 1, NGC 6337, Sp 1) – stars: AGB and post-AGB

Online-only material: color figures

1. INTRODUCTION

Planetary nebulae (PNe), which represent the near-ends of the lives of intermediate-mass (∼1–8 $M_\odot$) stars, afford insight into the late stages of stellar evolution. As an asymptotic giant branch (AGB) star sheds its tenuous envelope, it unveils a hot (T up to $\gtrsim 10^5$ K) core that is capable of ionizing the surrounding material and will eventually evolve into a white dwarf (WD). PNe are well known for their wide variety of optical emission line morphologies; this morphological diversity reflects the effects of energetic, nebula-shaping wind collisions. Recently, X-ray observations of PNe have shed light on the processes within nebular interiors, as well as on the properties of their central stars, that directly relate to PN shaping (for a review, see Kastner et al. 2012, hereafter Paper I).

Models describing the structure of PNe (Kwok et al. 1978; Schmidt-Voigt & Koppen 1987; Marten & Schönberner 1991; Villaver et al. 2002; Perinotto et al. 2004; Toalá & Arthur 2014)

posit that fast ($v_w \simeq 500$–$1500\,\mathrm{km\,s^{-1}}$) winds emanating from the pre-WD will collide with the previously ejected AGB envelope, sweeping up the AGB ejecta into a thin shell. These wind collisions result in shocks that heat the fast wind gas to temperatures $>10^6$ K, creating a "hot bubble" capable of producing soft X-rays (0.3–1 keV). A binary companion to the central star of the PN (CSPN) is capable of further influencing the PN shape via the formation of an accretion disk (Soker & Rappaport 2000), the transfer of angular momentum, the generation of a strong magnetic dynamo at the CSPN (Nordhaus et al. 2007), or, in the case of a close binary, the formation of jets (Soker & Livio 1994; Miszalski et al. 2011; Corradi et al. 2011; Boffin et al. 2012; Tocknell et al. 2014). While some CSPNe with hot photospheres ($\gtrsim 100$ kK) are capable of emitting soft X-rays, many CSPNe exhibit hard X-rays (>1 keV) that cannot be attributed to photospheric emission alone (Montez & Kastner 2013; Montez et al. 2014). Such hard X-rays might be expected, however, when a hot, compact companion accretes material, as suggested for some WDs with hard X-ray emission (Bilíková et al. 2010), or from the corona of a "rejuvenated" late-type companion of a post-common envelope binary CSPN (Montez et al. 2010). There is also the possibility that a "hard excess" could result from material infall from a debris disk around the CSPN, similar to the debris disk discovered around the central star of the Helix Nebula and possibly linked to its hard X-ray emission (Su et al. 2007). Alternatively, the hard X-ray emission might emerge from shocks within the stellar wind, via a process similar to that observed in O and B stars (Cassinelli et al. 1994).

The *Chandra* Planetary Nebulae Survey (CHANPLANS) is designed to place constraints on the frequency of the appearance and range of X-ray spectral characteristics of X-ray-emitting PN central stars and the evolutionary timescales of wind-shock-heated bubbles within PNe. The initial CHANPLANS program consisted of observations of 21 high-excitation PNe selected from among the ∼120 known PNe within ∼1.5 kpc of Earth, along with another 14 PNe previously observed by *Chandra* that fall within this volume (Paper I). The initial results included more than a dozen new detections of X-ray point sources and placed new constraints on the physical conditions, timescales, and frequency of hot bubbles. The survey recently continued with a 670 ks *Chandra* Cycle 14 Large Program of an additional 24 compact ($R_{\rm neb} \lesssim 0.4$ pc) PNe selected from among the volume-limited sample. In this paper, we describe the results of the CHANPLANS survey observations of these compact PNe in the context of the overall volume-limited sample of PNe. In two companion papers (Montez et al. 2014, 2014, in preparation), we detail the characteristics of point-like and diffuse X-ray emission sources within PNe, and further examine the origins and implications of these PN X-ray sources.

2. OBSERVATIONS AND DATA REDUCTION

2.1. Sample: Compact ($R_{\rm neb} \lesssim 0.4$ pc) Planetary Nebulae within ∼1.5 kpc

The PNe that constitute the sample observed with *Chandra* during Cycle 14, listed in Table 1, were primarily selected so as to further probe the onset, evolutionary timescale, and properties of diffuse X-ray sources within PNe. Hence, we selected objects on the basis of their relatively small physical dimensions, as ascertained via optical imaging. More specifically, we chose the 24 Table 1 objects from the compilation of solar-neighborhood PNe in Frew (2008) such that the resulting merged Cycle 12+14+archival sample would constitute a representative

volume-limited ($D \lesssim 1.5$ kpc) sample of PNe with inner bubble or inner shell radii $\lesssim 0.4$ pc (excluding very low surface brightness PNe, which typically have faint central stars). We estimate that our completeness in surveying compact ($R_{\rm neb} \lesssim 0.4$ pc) nebulae within ∼1.5 kpc is 90%, based on the solar neighborhood census of PNe recently compiled by Frew et al. (2014b). The chosen nebular radius roughly corresponds to a dynamical PN lifetime of $\lesssim 10^4$ yr—approximately twice the apparent hot bubble dissipation timescale inferred from Cycle 12 plus archival *Chandra* data shown in Paper I—assuming typical PN expansion velocities of ∼40 km s^{-1} (Jacob et al. 2013). Basic PN and CSPN data for the sample objects can be found in Table 1.

2.2. Observations

All Cycle 14 PNe were observed with the back-illuminated (BI) CCD S3 of *Chandra*'s Advanced CCD Imaging Spectrometer (ACIS). The use of CCDs as X-ray detectors provides determinations of incident photon energies as well as locations, which in turn allows for filtering of images by photon energy. *Chandra*/ACIS-S3 has an energy sensitivity of ∼0.3–8.0 keV, with a field of view of ∼8′ × 8′ and a pixel size of 0″.492. The BI CCD S3 has greater low-energy (<1 keV) sensitivity compared to the front-illuminated ACIS-I array, extending sensitivity down to ∼0.2 keV for high soft photon fluxes, albeit with uncertain calibration (Montez & Kastner 2013). Additionally, the use of S3 facilitates subpixel event repositioning (SER) in processing so as to better sample the core of the point spread function generated by *Chandra*'s High-Resolution Mirror Assembly (Li et al. 2004). Observation IDs, dates, and exposure times for the Cycle 14 CHANPLANS observations are listed in Table 2.

2.3. Data Reduction

All data were reduced using CIAO[24] (version 4.5). Data reduction made use of the CHANPLANS pipeline, which is detailed in Paper I. Briefly, this pipeline consists of processing the following steps: reprocessing of the primary and secondary data files and the application of SER using `chandra_repro`; detection of sources in the full field of view of each observation using `wavdetect`; calculation of statistics from a 3″.5 radius region centered on the CSPN, to place constraints on possible X-ray point source emission; and generation of annotated two-panel images displaying a filtered *Chandra* X-ray image highlighting the predominantly soft X-ray (0.3–2.0 keV) nature of the nebulae and the best available optical (Hα or *R* band) image obtained from the *Hubble* Legacy Archive,[25] the Wisconsin-Indiana-Yale-NOAO (WIYN) 0.9 m telescope (see Paper I), the SuperCOSMOS H-Alpha Survey (Parker et al. 2005; Frew et al. 2014a), or the Digitized Sky Survey (DSS[26]), as indicated in the panels (Figure 1).

3. RESULTS

Results from the Cycle 14 *Chandra* observations listed in Table 2 are illustrated in Figures 1–3 and are summarized in Tables 1 and 3. The last column of Table 1 indicates whether the PN was detected and, if so, the type of X-ray emission detected (point-like, diffuse, or both). As in Paper I, our conservative estimate for our sensitivity limits for diffuse and hard (soft) point-like X-ray sources are ∼10^{30} and ∼10^{29} (∼10^{31}) erg s^{-1},

---

Table 1
Planetary Nebulae within 1.5 kpc[a] Observed by *Chandra*

Name	PN G	Morph.[b] (F08/SMV11)	D (kpc)	R_{neb} (pc)	Age (10^3 yr)	T_* (kK)	Sp. Type	Comp.[c]	H$_2$[d]	X-Rays[e]
A65	017.3−21.9	Eafm:/Ls	1.17	0.30	17.5[f]	114[g]	O(H)	(Y)	. . .	N
HaWe 13	034.1−10.5	Efp?/Esip	1.01	0.18	. . .	68	hgO(H)	. . .	. . .	N
Hb 5	359.1−00.9	Bps/Bcbmph	1.70	0.13	1.5[h]	172	. . .	. . .	Y	D
HbDs 1	273.6+06.1	Er?/Is	0.80	0.29	. . .	119[i]	O(H)	. . .	. . .	P
He 2-11	259.1+00.9	Ebps/Bcbsip	1.14	0.24	0.7[j]	108[j]	. . .	K5V[j]	. . .	N
IC 1295	025.4−04.7	Efm:/Es(b/ti)	1.23	0.30	11	98	hgO(H)	. . .	. . .	N
IC 2149	166.1+10.4	E/Bsh	1.52	0.04	2	42	Of(H)	. . .	N	N
IC 4637	345.4+00.1	Eam/Estp	1.30	0.05	2	50	O(H)	(Y?)	. . .	N
IC 5148/50	002.7−52.4	Rm/Rsiph	0.85	0.27	5	110	hgO(H)	. . .	. . .	N
M 1-26	358.9−00.7	R/Mcbsih	1.20	0.02	1	33	Of(H)	. . .	. . .	N
M 1-41	006.7−02.2	Bs/(I/B)	1.47	0.15	. . .	187	. . .	. . .	Y	N
NGC 1501	144.5+06.5	Es/Esph	0.72	0.09	2	135	[WC4]	. . .	. . .	D
NGC 2899	277.1−03.8	Baps/Bosbp	1.37	0.37	14	215[k]	. . .	F5V:	Y	N
NGC 3918	294.6+04.7	Ems(h)/Lsbairh	1.84	0.08	3	150	O(H)?	. . .	. . .	D
NGC 6026	341.6+13.7	Ef/Ish	1.31	0.16	6	35	O7(H)	WD?	. . .	N
NGC 6072	342.1+10.8	Ba/Mcot	1.39	0.23	23	140	. . .	. . .	Y	N
NGC 6153	341.8+05.4	Es/Esah	1.10	0.07	4	109	Of(H)?	. . .	N	D
NGC 6337	349.3−01.1	Epr/Rsarh	0.86	0.10	12	105	. . .	(Y)	. . .	P
NGC 6369	002.4+05.8	Ebpr(h:)/Mcst	1.55	0.12	3	66	[WO3]	. . .	Y	D
NGC 6894	069.4−02.6	Emr/Eh	1.31	0.17	4	100	. . .	. . .	. . .	N
NGC 7076	101.8+08.7	Ea/Esh	1.47	0.20	5	80	. . .	. . .	. . .	N
NGC 7354	107.8+02.3	Emp/Esaph	1.60	0.09	3	96	. . .	. . .	N	N
Sh 2-71	035.9−01.1	Bs/Lsbp	1.14	0.30	14	157	. . .	. . .	N	N
Sp 1	329.0+01.9	Rr/Rsh	1.13	0.20	6	72	O(H)	(Y)	. . .	P

Notes.

[a] PN and central star data compiled from (Frew 2008, and references therein) unless otherwise noted.

[b] Morphologies as listed in Frew (2008, F08): B: bipolar, E: elliptical, R: round, a: asymmetry present, b: bipolar core present, f: filled (amorphous) center, m: multiple shells present, p: point symmetry present, r: ring structure dominant, s: internal structure noted, (h): distinct outer halo. Morphologies following an abbreviated and very slightly modified version of the classification system described in Sahai et al. (2011) (SMV11; see their Table 2): B: bipolar, M: multipolar, E: elongated, I: irregular, R: round, L: collimated lobe pair, S: spiral arm, c: closed outer lobes, o: open outer lobes; s: CSPN apparent, b: bright (barrel-shaped) central region, t: bright central toroidal structure; p: point symmetry, a: ansae, i: inner bubble, h: halo; r: radial rays; (/): alternate possibilities.

[c] "(Y)" = known binaries with unknown companion types; "(Y?)" = possible binary; otherwise the type of the companion star is as listed (De Marco 2009).

[d] "Y" = near-IR H$_2$ detected; "N" = near-IR H$_2$ not detected (Bernard-Salas & Tielens 2005; Bohigas 2001; Webster et al. 1988; Ramos-Larios et al. 2013; Kastner et al. 1996, and references therein).

[e] X-ray results key: P = point source; D = diffuse source; N = not detected.

[f] Huckvale et al. (2013).

[g] Hillwig et al. (2014).

[h] López et al. (2012).

[i] Herald & Bianchi (2011).

[j] Jones et al. (2014a).

[k] Drew et al. (2014).

respectively, at a distance of 1.5 kpc. We will revisit these sensitivity limits in Montez et al. (2014, 2014, in preparation).

Table 4 (an update of Table 4 from Paper I) lists X-ray detection statistics broken down by PN morphology, H$_2$, detection/non-detection fraction, and known central star binarity for the entire CHANPLANS sample. Figures 3 and 4 are updates of Figures 5 and 6, respectively, in Paper I. In Figure 3, various observed parameters for the sample PNe—optical morphology, H$_2$ detection/non-detection, X-ray detection/non-detection, and X-ray source type—are illustrated in a plot of CSPN effective temperature versus nebular radius. In Figure 4, we plot median X-ray photon energy against nebular radius. In Figure 5, which has no counterpart in Paper I, we further illustrated PN X-ray detections and non-detections in the form of plots of PN distances and ratios of [O III] to Hβ fluxes against nebular densities for all (59) CHANPLANS sample PNe.

3.1. Cycle 14 Detections of X-Rays from PNe

We have detected five of the Table 1 PNe in diffuse X-ray emission: Hb 5, NGC 1501, NGC 3918, NGC 6153, and NGC 6369 (Figure 2). The last four objects are detected for the first time; Hb 5 was detected previously by *XMM-Newton* (Montez et al. 2009, see below). These detections represent a ∼21% (5/24) detection rate of hot bubbles within the Cycle 14 sample. When these detections are combined with the previous CHANPLANS observations, the CHANPLANS detection rate of PNe hot bubbles now stands at ∼27% (16/59). Two of the newly detected objects, NGC 1501 and NGC 6369, host Wolf-Rayet-type (WR) CSPNe, which brings the CHANPLANS diffuse detection rate of such objects to 100% (5/5). The detection rate of diffuse X-ray emission from [WR]-type CSPNe remains high when including PNe beyond ∼1.5 kpc (see Kastner et al. 2008). These diffuse X-ray detections follow the previously established trend that diffuse X-ray PNe generally display compact ($R_{neb} \lesssim$ 0.15 pc), elliptical optical morphologies (Figure 3; Paper I). A notable exception is Hb 5, which has a bipolar morphology.

The detections of X-ray point sources within three Cycle 14 PNe, HbDs1, NGC 6337, and Sp 1 (Table 1) yielded a ∼13% detection rate of CSPNe. These Cycle 14 detections bring the overall CHANPLANS detection rate of CSPNe to ∼36% (21/59).
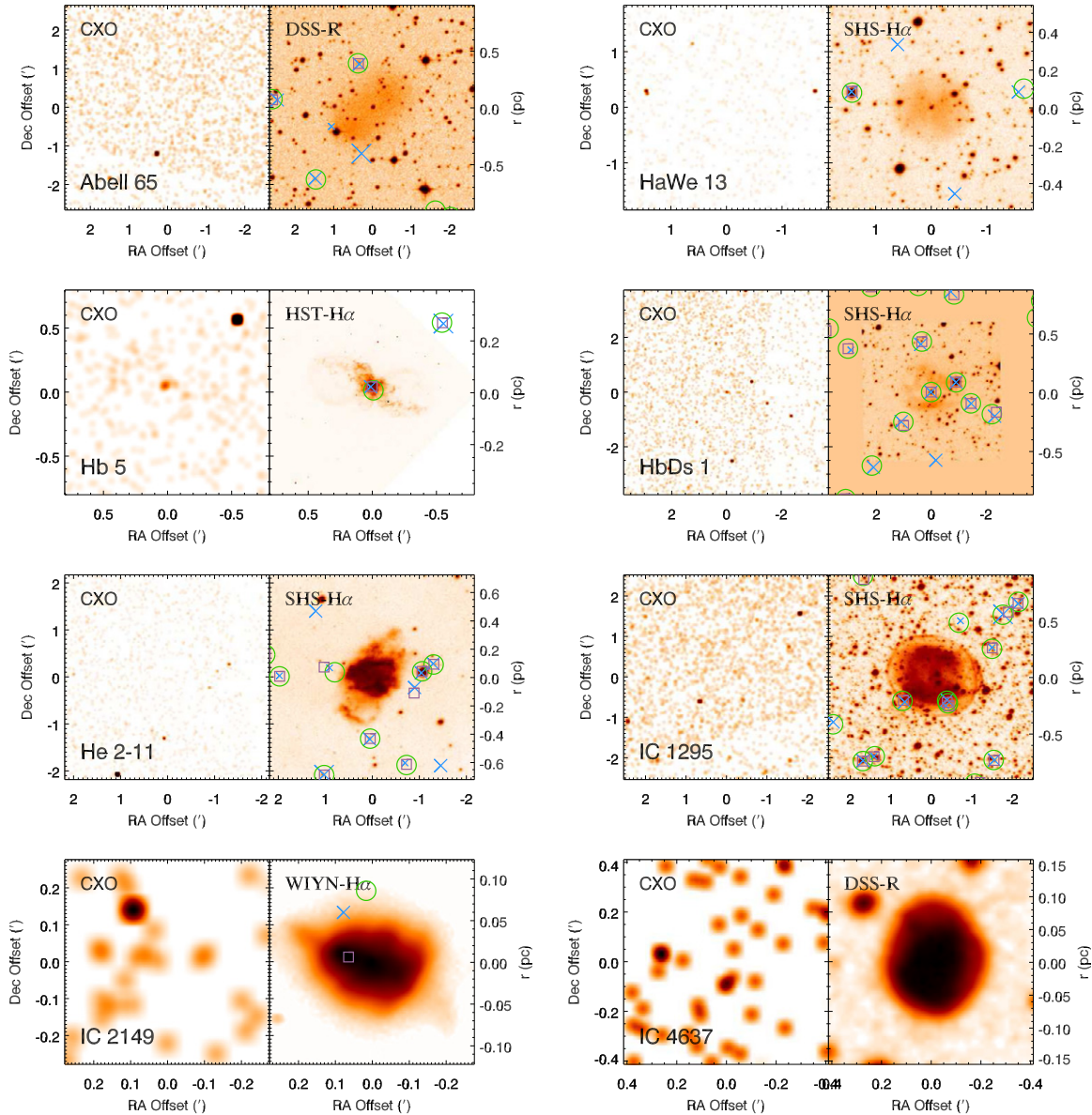
Figure 1. CHANPLANS pipeline output for the Table 1 PNe. Two panels are presented for each PN. The left panel of each pair shows the *Chandra*/ACIS soft-band (0.3–2.0) keV image, smoothed with a Gaussian function with $3''$ FWHM ($1''$ FWHM for M 1-26, or $6''$ FWHM for images larger than $5'$ on a side), centered on the SIMBAD coordinates of the PN (which lies on back-illuminated CCD S3). The right panel shows an optical image (obtained from *HST*, WIYN, the SuperCOSMOS H-alpha Survey, or the DSS, as indicated) overlaid with the positions of detected broad-band (0.3–8.0 keV) X-ray sources (crosses), USNO catalog stars (circles), and 2MASS Point Source Catalog IR sources (squares). The size of the cross is proportional to the number of X-ray photons detected.
(A color version of this figure is available in the online journal.)

Two of the three new CSPNe detections (within NGC 6337 and Sp 1) are known binaries, which brings the overall CHANPLANS detection rate of all CSPN that are known to be binaries (at the time this paper was written) to 60% (Table 4).

3.2. PNe Displaying Diffuse X-Ray Emission

The diffuse X-ray emitting PNe detected in the Cycle 14 sample are displayed in Figure 2 and are briefly described below. As is evident in Figures 3 and 4 and Table 4, these detections reinforce previous CHANPLANS results indicating that PNe displaying diffuse X-rays are predominantly elliptical in morphology with $R_{\rm neb} \lesssim 0.15\,{\rm pc}$; furthermore, diffuse X-ray PNe generally lack detections of near-IR H_2 emission. In a forthcoming paper (R. Montez et al. 2014, in preparation), we present a global analysis of the CHANPLANS diffuse X-ray

sources. Here, we describe the properties of the diffuse X-ray PNe detected during Cycle 14 observations.

3.2.1. Classical Hot Bubbles

NGC 3918 appears to host multiple shells, and is similar in optical and X-ray morphology to multiple-shell, diffuse X-ray PNe such as NGC 6543 (Paper I). Three-dimensional models of the nebula vary in their interpretations of its morphology. Clegg et al. (1987) modeled NGC 3918 as a biconical nebula within an optically thin sphere, while a spindle-like structure was favored by both Corradi et al. (1999) and Ercolano et al. (2003). Like NGC 1501, the shell of the nebula shows enhanced [O III]/Hα emission resulting from the inner shell expanding into the outer shell (Guerrero et al. 2013), while the inner shell confines the diffuse X-ray emission.
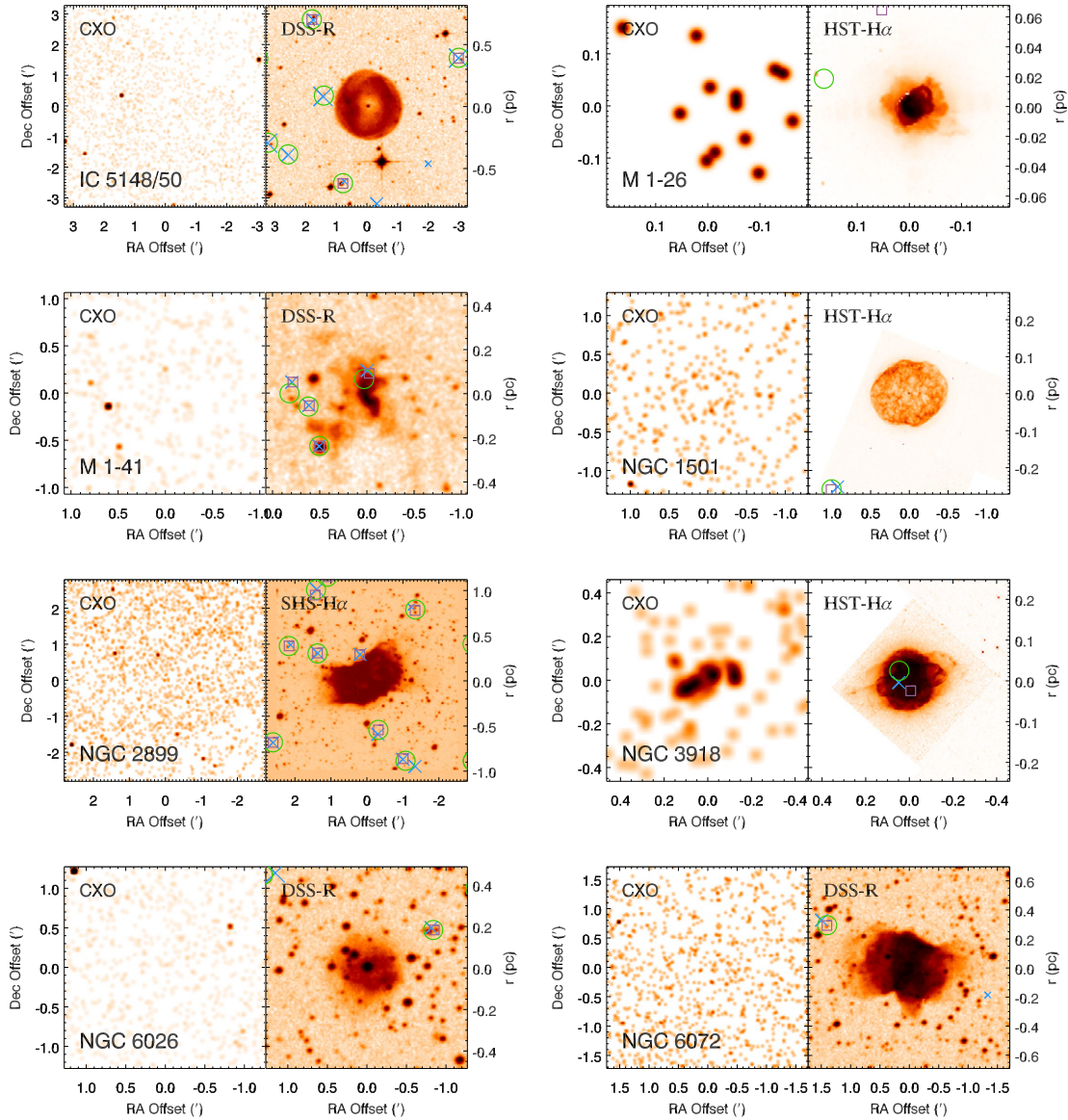
Figure 1. (Continued)

NGC 6153 is also an elliptical nebula that hosts multiple shells, and is thought to be the product of a high-mass (4.5 $M_\odot$) progenitor (Pottasch & Bernard-Salas 2010). Often compared to NGC 7009, NGC 6153 is indeed morphologically similar, both in the optical and X-ray; however, NGC 6153 lacks the ansae found in NGC 7009. The diffuse X-ray emission is confined to the inner shell, as is the case with NGC 3918 and similar multiple-shell, diffuse X-ray PNe (Paper I).

3.2.2. PNe with [WR]-type CSPNe

Both NGC 1501 and NGC 6369 harbor [WR]-type central stars and diffuse X-ray emission. NGC 1501 is an elliptical nebula with a [WR]-type central star within a complex, filamentary internal structure. The central star has been reclassified many times between [WO] and [WC] type. Based on emission lines detected in the optical spectrum, the CSPN appears to be [WO4] (Crowther et al. 1998; Ercolano et al. 2004); however, the star also displays an infrared excess from J through all *Spitzer* IRAC bands, which is indicative of circumstellar dust, as is common

for [WC]-type stars (Bilíková et al. 2012). NGC 1501 shows enhanced [O III]/Hα emission along the surface of the nebular shell, which is evidence for shocks along the skin (Guerrero et al. 2013). Similarly, the X-ray emission appears to trace shocks inside the primary nebular shell.

In contrast to the elliptical shell and filamentary internal structure of NGC 1501, NGC 6369 appears to have a spherical main nebular shell described as a barrel, with bipolar outflows (Ramos-Larios et al. 2012). This structure is similar to that of NGC 40 (Montez et al. 2005). Where [O III] and Hα are dim in NGC 6369, the nebula is bright in [N II], displaying a ring of emission along the inner shell. The bright optical shell is filled with H_2 and surrounded by a photodissociation region (Ramos-Larios et al. 2013), and the shell encloses the diffuse X-ray emission around the [WO]-type central star (Peña et al. 2013). The correspondence of the X-ray emission and the nebular shell, and lack of emission from the blowouts, suggests that emission is generated by the strong winds of the CSPN colliding with the progenitor red giant wind, as is the case for NGC 40 (Montez et al. 2005).
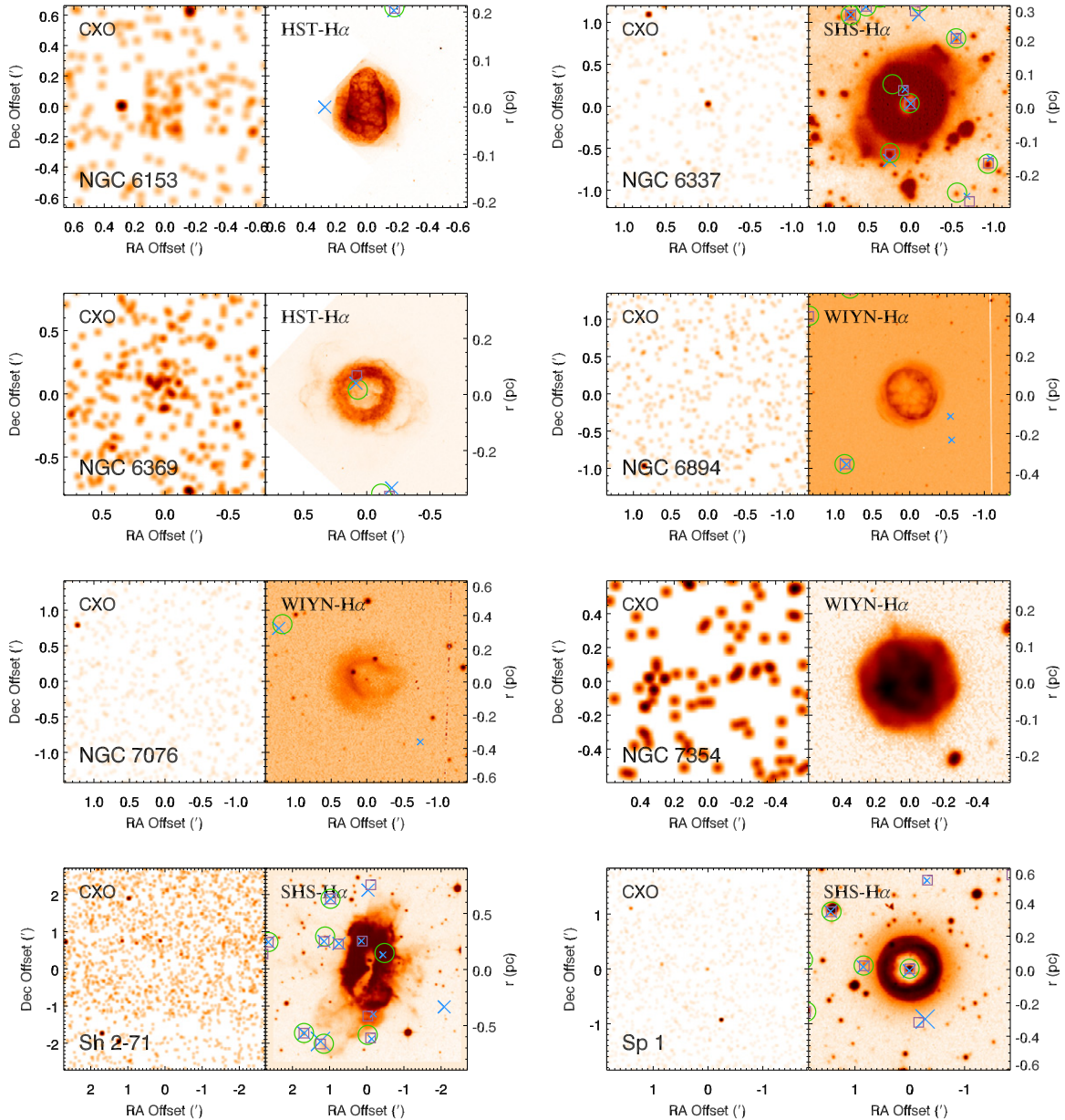
Figure 1. (Continued)

3.2.3. The Bipolar Planetary Nebula, Hb 5

Hb 5 is a bipolar nebula with large lobes (∼27″) extending east and west and a tight waist with a bright core that contains secondary expanding lobes. The smaller lobes (≲12″) may result from an interaction between a fast, low-density wind and an inhomogeneous, high-density circumstellar shell (López et al. 2012). Diffuse X-ray emission was previously detected serendipitously by *XMM-Newton* (Montez et al. 2009). The emission in the *XMM* images appeared coincident with the peak optical emission around the core and possibly along the Hα emission in the lobes, although *XMM*'s resolution was insufficient to determine if the X-ray emission is extended.

The Cycle 14 *Chandra* observations of Hb 5 also yielded the detection of a bright, compact X-ray core, coincident with the peak optical emission. There is no apparent X-ray point source from the CSPNe contributing to the core emission. Additionally, X-ray emission was tentatively detected along the tip of the eastern lobe, which appears blueshifted, while no apparent emission is seen from the western, redshifted lobe, which may be attributed to extinction by intervening nebular material (López et al. 2012).

### 3.3. PNe Displaying Point-like X-Ray Emission at Central Stars

The three Cycle 14 X-ray point source detections (HbDs1, NGC 6337, Sp 1) continue the trend, noted in Paper I, that soft (∼0.6–1.0 keV) X-ray sources likely indicate the presence of CSPN photospheric emission and/or wind shocks, while hard (≳1.0 keV) sources appear related to the presence of binary companions to CSPNe (Figure 4; R. Montez et al. 2014a, in preparation). Below are brief summaries of each of the Table 1 PNe with newly detected point-like X-ray emission.

HbDs1 is an irregularly elliptical nebula around the hot blue star LSS 1362 (T_{eff} = 116 kK; Herald & Bianchi 2011).
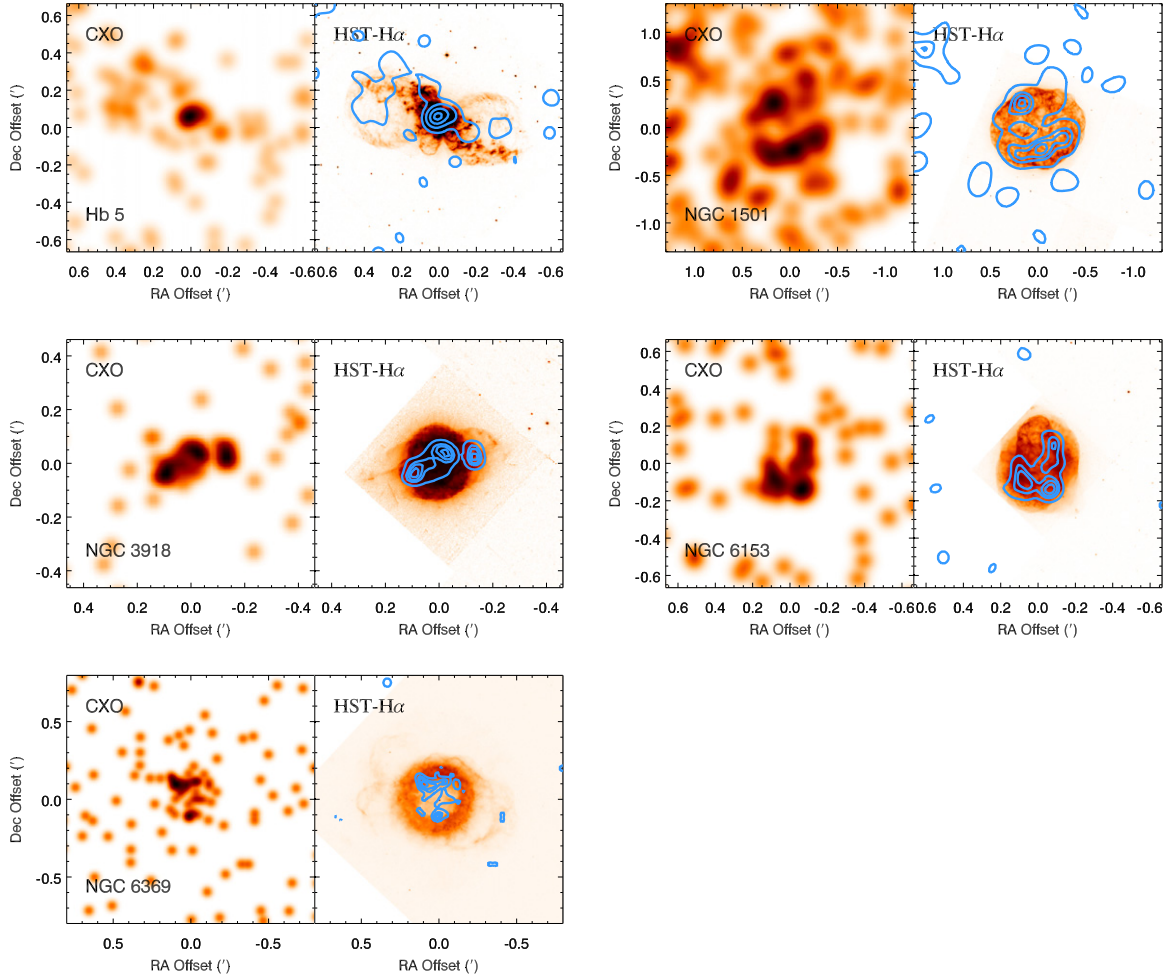
Figure 2. Images of Table 1 PNe in which diffuse X-ray emission has been detected by *Chandra*. The left and right panel for each PN display, respectively, *Chandra* 0.5–1.2 keV images filtered to efficiently remove the soft background and *Chandra* contours overlaid on optical images. The *Chandra* images of Hb 5, NGC 1501, and NGC 6153 have been smoothed with a 12″5 FWHM Gaussian, while the *Chandra* images of NGC 3918 and NGC 6369 have been smoothed with a FWHM of 3″. The contour levels of all but Hb 5 are 30%, 60%, 75%, and 90% of the maximum X-ray surface brightness (Hb 5 has contour levels of 10%, 30%, 60%, and 90%).

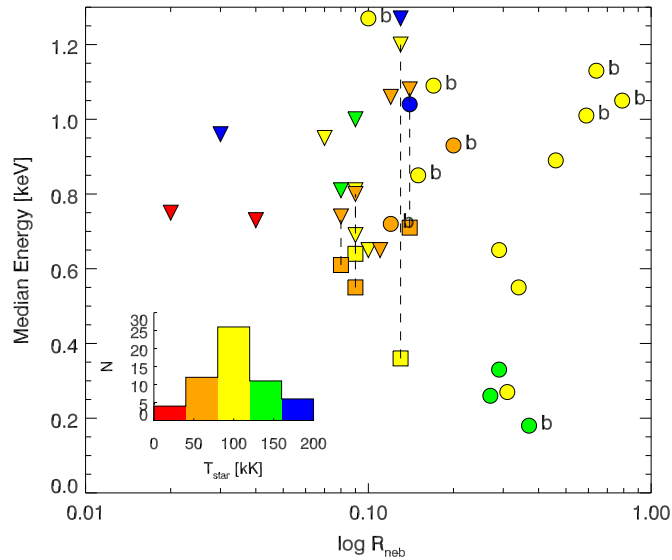(A color version of this figure is available in the online journal.)
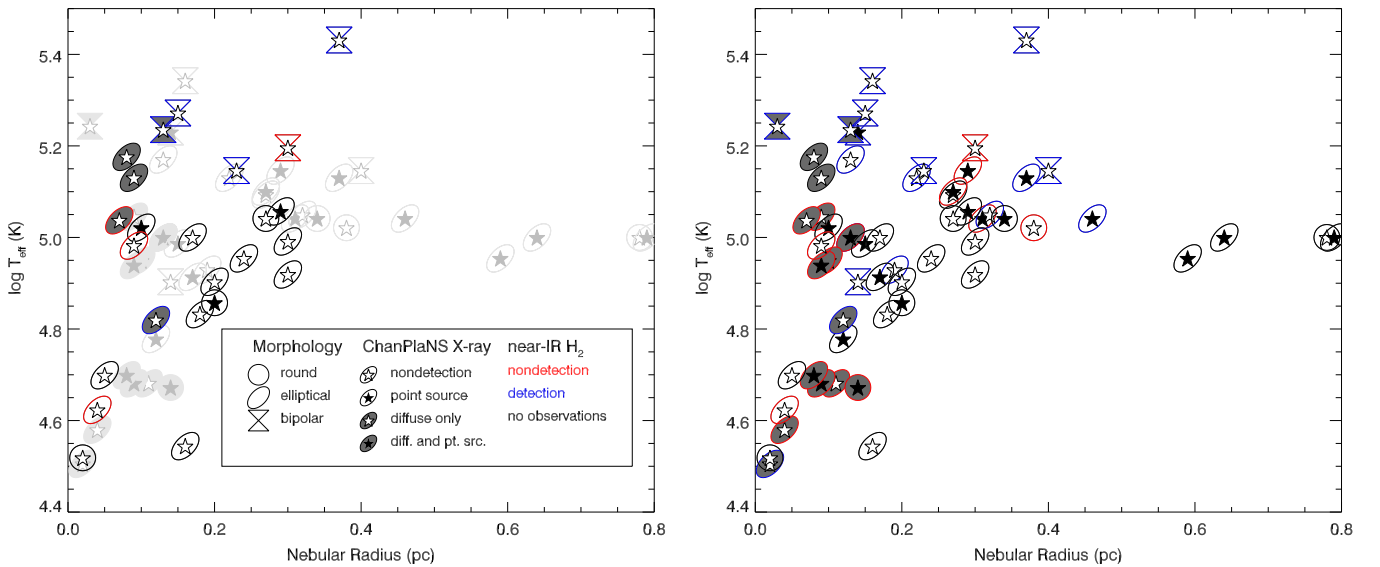
Figure 3. Plots of CSPN T_{eff} vs. PN radius for all ChanPlaNS observed objects, with symbols indicating the presence or absence of diffuse or point-like X-ray emission, as well as PN morphology and the presence or absence of H_2 emission. In the left panel, the highlighted objects represent Cycle 14 data and the light gray objects represent Cycle 12 and archival data (Paper I).

(A color version of this figure is available in the online journal.)

Table 2
Log of *Chandra* Observations

Name	OBSID	Date	Exposure (ks)
A65	14583	2013 Aug 22	29.7
HaWe 13	14578	2013 Jul 15	18.6
Hb 5	14596	2013 Oct 18	29.1
HbDs 1	14575	2013 Aug 10	19.5
He 2-11	14581	2013 Aug 10	29.6
IC 1295	14585	2013 Aug 04	29.7
IC 2149	14593	2012 Dec 30	28.7
IC 4637	14586	2014 Mar 08	29.6
IC 5148/50	14576	2013 Apr 07	19.7
M 1-26	14584	2013 Aug 10	29.6
M 1-41	14591	2013 Mar 02	29.6
NGC 1501	14574	2012 Dec 08	19.7
NGC 2899	14589	2013 May 28	29.6
NGC 3918	14597	2013 Jul 31	30.0
NGC 6026	14588	2013 Jun 29	29.6
NGC 6072	14590	2014 Jan 23	29.6
NGC 6153	14579	2014 Jan 17	28.6
NGC 6337	14577	2013 Aug 04	19.7
NGC 6369	14594	2013 Feb 18	29.6
NGC 6894	14587	2013 Dec 13	29.2
NGC 7076	14592	2013 Mar 29	29.6
NGC 7354	14595	2013 Dec 26	29.6
Sh 2-71	14582	2013 Oct 07	29.6
Sp 1	14580	2013 Jan 24	29.4

Table 3
Planetary Nebulae X-Ray Point Source Characteristics

Name	N^a (photons)	C^b (ks^{-1})	Median E^c (keV)	E Range^d (keV)
A65[e]	1	0.02 ± 0.05	0.96	0.96–1.09
HaWe 13	. . .	<0.21	. . .	. . .
Hb 5[f]	15:	0.51 ± 0.09:	0.94:	0.81–1.03
HbDs 1	10	0.49 ± 0.06	0.65	0.56–0.78
He 2-11	. . .	<0.14	. . .	. . .
IC 1295	. . .	<0.13	. . .	. . .
IC 2149	. . .	<0.14	. . .	. . .
IC 4637	. . .	<0.14	. . .	. . .
IC 5148/50	. . .	<0.20	. . .	. . .
M 1-26	. . .	<0.15	. . .	. . .
M 1-41	. . .	<0.14	. . .	. . .
NGC 1501[g]	. . .	<0.20:	. . .	. . .
NGC 2899	. . .	<0.14	. . .	. . .
NGC 3918[g]	21:	0.71 ± 0.06:	0.85:	0.66–1.03
NGC 6026[e]	1	0.05 ± 0.08	1.16	0.90–2.31
NGC 6072	. . .	<0.14	. . .	. . .
NGC 6153[g]	. . .	<0.14:	. . .	. . .
NGC 6337	39	1.99 ± 0.07	1.27	1.03–1.73
NGC 6369[g]	8:	0.27 ± 0.07:	1.06:	0.96–2.38
NGC 6894	. . .	<0.14	. . .	. . .
NGC 7076	. . .	<0.14	. . .	. . .
NGC 7354	. . .	<0.14	. . .	. . .
Sh 2-71	. . .	<0.14	. . .	. . .
Sp 1	11	0.37 ± 0.07	0.93	0.83–1.33

Notes.
[a] Number of source photons, after background subtraction.
[b] Source photon count rate.
[c] Median source photon energy.
[d] Source photon energy range (25th through 75th percentiles).
[e] Uncertain point source detections at the positions of known binaries. See Section 3.3.
[f] There is no point source apparent within Hb 5.
[g] Point source counts, count rate (or upper limit), median energy, and energy ranges are uncertain due to presence of diffuse emission component.

Table 4
Planetary Nebulae: *Chandra* X-Ray Detection Statistics

| Category^a	N^b	$N_{PX}{}^c$	$N_{DX}{}^c$
Entire sample	59	21 (36%)	16 (27%)
Round/elliptical, F08	47	19 (40%)	14 (30%)
Bipolar, F08	12	2 (17%)	2 (17%)
Round/elliptical/irregular, SMV11	37	14 (38%)	9 (24%)
Bipolar/multipolar, SMV11	22	7 (32%)	7 (32%)
Near-IR H$_2$ not detected	19	9 (47%)	10 (53%)
Near-IR H$_2$ detected	18	3 (17%)	4 (22%)
Known binary CSPN	19	11 (58%)	2 (11%)

Notes.
[a] Morphologies as listed and defined in Column 3 of Table 1 and associated footnotes; CSPN binary detections and H$_2$ detections as listed, respectively, in Columns 9 and 10 of Table 1.
[b] Total number of sample PNe in each category.
[c] Number of PNe in each category displaying point-like and/or diffuse X-ray emission in *Chandra* imaging (Paper I).

Figure 4. Median X-ray photon energy vs. nebular radius for all Cycle 12+14+archival sample PNe detected as X-ray sources. Symbol shapes indicate the nature of the PN X-ray source (triangles: diffuse sources; circles: CSPN point sources; squares: diffuse+CSPN sources) and are color-coded according to CSPN T_{eff}, whose distribution for the observed sample is shown in the inset histogram. Known binary CSPNe are indicated by "b." The dashed line connects the diffuse+CSPN emission with the corresponding diffuse emission for sources that exhibit both types of emission.

(A color version of this figure is available in the online journal.)

The nebula has enhanced Hα emission along its northern and southern limbs. The magnetic field properties of the CSPN have been debated. A kG field was inferred by Jordan et al. (2005, 2012) from spectropolarimetric data taken with the ESO Very Large Telescope; however, more recent FORS2 observations showed no evidence of such a strong field (with upper limits of $B < 600$ G; Leone et al. 2011; Bagnulo et al. 2012).

The detected X-ray point source has a median energy of 0.65 keV, which may indicate self-shocking within the stellar winds previously detected at the CSPN (Herald & Bianchi 2011; Guerrero & De Marco 2013), possibly combined with photospheric emission (see Montez & Kastner 2013).
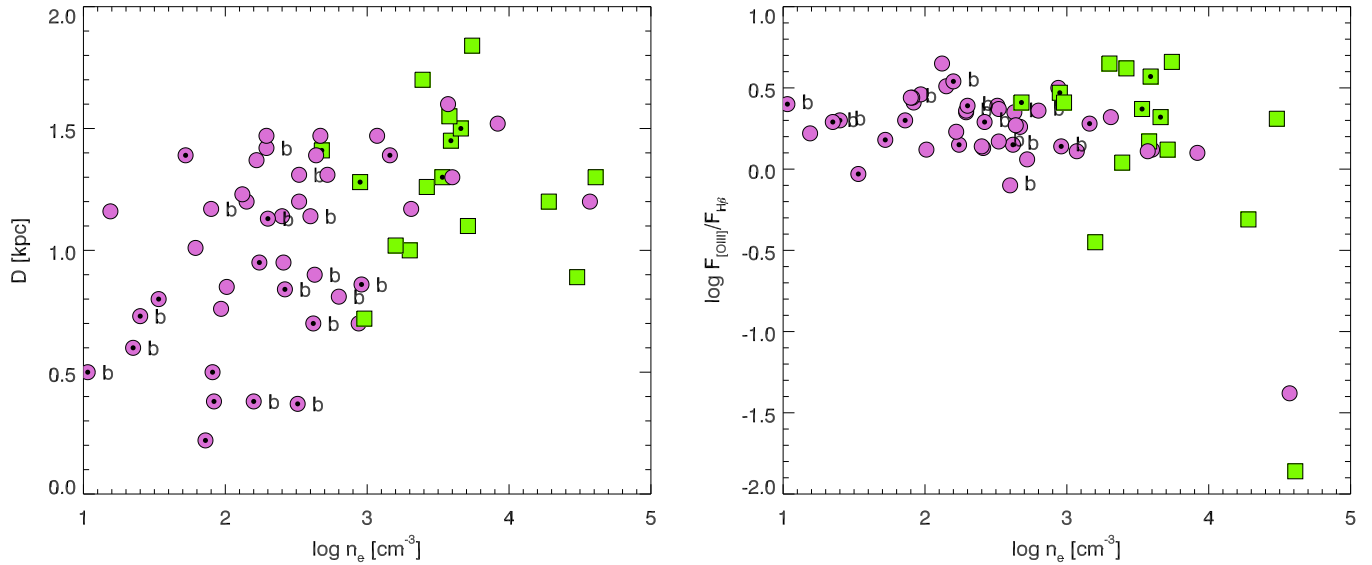
Figure 5. Distance (left) and ratio of [O III] to Hβ fluxes (right) vs. the log of electron density n_e for PNe detected (green squares) and not detected (purple circles) as CHANPLANS diffuse X-ray sources. A bullet within each symbol indicates that the CSPNe was detected as a point-like X-ray source. A "b" next to a symbol indicates the CSPN is a known binary.

(A color version of this figure is available in the online journal.)

NGC 6337 is seen as a ring nebula with radial filaments. This PN harbors a nearly face-on ($i \lesssim 15°$) close binary (0.17 day period) central star system (Hillwig et al. 2010). It is likely that the nebula is viewed nearly pole-on as well, suggesting a bipolar structure with a narrow waist around the binary (García-Díaz et al. 2009). The close binary is most likely the product of a common envelope phase (De Marco et al. 2011), leaving behind a pre-WD and a cool main-sequence star (Hillwig et al. 2010). The X-ray point source associated with this binary has a median energy of 1.27 keV, the hardest emission detected from a point source in the CHANPLANS sample thus far. This hard X-ray detection provides strong support for a model in which the X-rays originate from a cool, coronally active companion (see Section 4).

Sp 1 appears similar to NGC 6337; this PN is also a diffuse ring on the plane of sky and harbors a close binary (2.9 day period) at its center (Bond & Livio 1990; Jones et al. 2012; Bodman et al. 2012). Spatiokinematical modeling of the nebular shell shows that the nebula is a nearly pole-on hourglass shape (Jones et al. 2012). This is borne out by modeling of the CSPN by Bodman et al. (2012), which indicates a G0 or F8 main sequence companion with an orbital inclination of $10° < i < 20°$, consistent with the generation of a near pole-on nebula. UV spectra of the CSPN show evidence for stellar winds (Patriarchi & Perinotto 1991), which could be at best partly responsible for the X-ray point source at the CSPN. However, the median energy for the X-rays from the Sp 1 CSPN is 0.93 keV, making it one of the harder X-ray sources in the CHANPLANS sample, and suggesting that the companion dominates the detected emission.

3.4. X-Ray Non-detections

Table 3 lists the point source X-ray characteristics (net counts, count rates, median photon energies, and photon energy ranges) of each PN in the Cycle 14 sample. To obtain these results, the 0.3–3.0 keV background counts were extracted from a source-free region near the central star. These background counts were scaled to the point source extraction radius of 3″.5, and then subtracted from the counts of the same extraction region centered on the CSPN, to obtain the net source counts (or source

count upper limits). Sources with less than six net counts are classified as undetected. Two sources lie below this background-subtracted limit, A65 and NGC 6026, but could be considered as tentative detections; there are ~4 (source+background) counts found near their CSPNe, both of which have companion stars. There are a few sources above the net count limit that we consider to be doubtful as point source detections: Hb 5, NGC 3918, and NGC 6369. Contamination from the diffuse X-ray emission in NGC 3918 makes it difficult to determine the contribution from a possible point source at the CSPN in the circular source region. NGC 6369 is a luminous, albeit reddened, PN that lies near the limit of our volume-limited sample, at a distance of 1.55 kpc (Monteiro et al. 2004). Additionally, the diffuse X-ray emission of NGC 6369 is not concentrated at the CSPNe, which makes it unlikely to contaminate a point source detection. Finally, as noted in Section 3.2, Hb 5 appears to have no point-like emission within the CSPN extraction region.

Several PNe that were undetected appear to fit within morphology trends typical of previous CHANPLANS point source and diffuse X-ray detections. IC 5148/50 is undetected, yet it has a morphology similar to Sp 1, suggesting that it may be a pole-on hourglass and, hence, could be the product of a binary system. In optical images, NGC 6894 has the multiple-shell structure of a hot bubble from which we would expect to see diffuse X-ray emission, though it is important to note that the central star is faint and on the WD cooling track. Similarly, NGC 7354 hosts multiple elliptical shells and ansae, similar to NGC 3918 and NGC 6153; however, no X-ray photons were detected from the innermost bubble of NGC 7354. These non-detections appear to place stringent limits on the timescales for X-ray emitting hot bubbles within PNe (Section 4.2)—although we note that NGC 7354 is quite heavily reddened and, hence, any soft X-rays from its interior might suffer considerable absorption.

The objects with no detectable X-ray emission have varying morphologies (round, elliptical, bipolar), with at least half exhibiting inherent asymmetries. IC 4637 is an example of a PNe that falls within the range of nebular properties for the diffuse X-ray detections (Paper I), but was not detected. Specifically,

9

IC 4637 has a radius of 0.05 pc and elliptical morphology (Frew 2008). Additionally, IC 2149 is a young, compact bipolar nebula with an elliptical central shell and may be the product of a low-mass progenitor and/or binary evolution (Vázquez et al. 2002). Upper limit estimates for X-ray luminosity L_X for each of these sources (R. Montez et al. 2014, in preparation) will help place constraints on the sizes, plasma densities, and morphologies of X-ray emitting nebulae.

4. DISCUSSION

The sample of 59 PNe within ∼1.5 kpc observed to date by *Chandra* constitutes a representative set of X-ray observations of mostly compact and, hence, predominately relatively young PNe within the solar neighborhood. Adding the 24 PNe observed in Cycle 14 to the initial sample (see Paper I) reduces the overall PN X-ray detection rate from ∼70% to ∼54% (32/59). This decrease most likely reflects the composition of the initial CHANPLANS sample; these objects were chosen based on the presence of bright excitation lines indicative of hot CSPNe ($T_{\rm eff} \gtrsim 10^5$ K) and/or structure that resulted from rapid evolution (Paper I), while the Cycle 14 objects were chosen to complete the X-ray census of compact ($R_{\rm neb} \lesssim 0.4$ pc) PNe within ∼1.5 kpc. Nevertheless, the Cycle 14 results underscore trends apparent in the X-ray properties of PNe, as we discuss in the following subsections.

4.1. Diffuse X-Ray Emission from [WR]-type CSPNe

The CSPNe that are H-deficient and display spectroscopic evidence for fast stellar winds and high mass-loss rates (up to 10^{-6} $M_{\odot}$ yr^{-1}; Crowther et al. 1998; DePew et al. 2011) are classified as [WR]-type because of their similarity, as a class, to luminous WR stars. The primary difference between the two classes is that the [WR]-type stars descend from intermediate mass (1–8 $M_{\odot}$) stars, whereas "classical" WR stars are the descendants of massive (>25–30 $M_{\odot}$) stars (Crowther et al. 2006). In total, there are five known [WR]-type CSPNe in the CHANPLANS sample: NGC 1501 and NGC 6369 from Cycle 14 (Table 1), as well as NGC 40, NGC 2371, and BD +30°3639 from Cycle 12 and archival observations (Paper I). All five of these [WR]-type CSPN objects display diffuse X-ray emission. The only consistent morphological similarity among all of the [WR] type CSPNe is that their main bubbles appear elliptical (Frew 2008). In each case, the diffuse X-ray emission is enclosed by the central optical bubble, although the morphology of the X-ray emission varies considerably from object to object.

BD +30°3639: The unusually bright, diffuse emission fills the central bubble, perhaps as a consequence of its very young age (∼10^3 yr; Frew 2008).

NGC 40: The emission appears within a partial ring that traces the inner edge of the bright optical rim of the nebula (Montez et al. 2005).

NGC 2371: The diffuse emission is contained within the bright nebular rim but does not seem to follow any significant optical feature, and is highly asymmetric.

NGC 1501: The X-ray emission traces the rim of the nebula, echoing the limb-brightened morphology of WR star wind-blown bubble S308 (Toalá et al. 2012).

NGC 6369: The diffuse emission is asymmetrical and strongest along the northern limb of the central bubble.

The X-ray results for most of the above PNe, with the possible exception of NGC 2371, reveal some potential similarities between PNe with [WR]-type CSPNe and the wind-blown

bubbles of massive WR stars. The X-ray limb-brightening in massive WR star wind-blown bubbles, such as S308, is the result of the hot WR wind cooling as it comes in contact with the previously ejected red (or yellow) supergiant or luminous blue variable material (García-Segura et al. 1996a, 1996b; Freyer et al. 2003; Toalá & Arthur 2011; Toalá et al. 2012; Dwarkadas & Rosenberg 2013). A similar process occurs in PNe, wherein the X-ray emission is contained within the ejected AGB envelope and does not come in direct contact with the ISM. The question remains: is the diffuse X-ray emission from [WR] CSPNe limb-brightened or not? Given the photon-starved nature of our detections, we will require Poisson-based models for comparison with the observations to adequately answer this question.

4.2. Diffuse X-Ray Emission and PN Size, Age, and Electron Density

The diffuse X-ray emission from hot bubbles in PNe is evidently confined to early phases in PN evolution. In Paper I, we pointed out that the central bubbles of PNe with diffuse emission tend to have elliptical, nested-shell morphologies and radii $\lesssim$0.15 pc (Figure 3 and Tables 1 and 4). This radius limit corresponds to dynamical ages $\lesssim$5 × 10^3 yr, roughly a quarter of the (21 ± 5) × 10^3 yr mean visibility time of PNe (Jacob et al. 2013). Our Cycle 14 detections and non-detections thereby reinforce the inference, made in Paper I, that diffuse X-ray emission is restricted to the most compact nebulae. We note that the correlation of diffuse X-rays with elliptical morphology is ambiguous (Table 4), but it remains the case that PNe with closed structures (whether bubbles or lobes) are more likely to be detected as diffuse X-ray sources.

Furthermore, from Figure 5 we see that with the exception of NGC 2371, all CHANPLANS PNe with diffuse X-ray emission have nebular densities $n_e \gtrsim 1000$ cm^{-3}, as determined via their Hα line luminosities and nebular radii, which are in turn determined from the Hα surface brightness versus radius relation (Frew 2008; Frew et al. 2014b). In contrast, the diffuse X-ray detection rate is essentially independent of distance and nebular excitation. Since PN density and radius are correlated, the remarkably sharp n_e boundary between diffuse X-ray detections and non-detections in Figure 5 further underscores the notion of a limit on the timescale for energetic (nebula-shaping) wind interactions in PNe. Moreover, Figure 5 suggests that, from the spectroscopy of density-sensitive lines (e.g., [O II], [S II]), it is possible to ascertain whether a PN might currently be in a wind-collision phase, when we would expect to see diffuse X-ray emission. Nevertheless, the duration of the wind-interaction phase is a complex problem that must account for (1) luminosity of the central star (e.g., Hb 5 high, NGC 5148 low), (2) expected hydrogen column density, and (3) spectral type of the central star (i.e., whether it is [WR] or not).

This density limit may explain the X-ray non-detection of nebulae like NGC 6894 and NGC 6804 (Paper I), which appear morphologically similar to known diffuse X-ray emitters. NGC 6894 has a nebular radius of 0.17 pc and NGC 6804 has a nebular radius of 0.19 pc, and both have a density $\log n_e \sim 2.7$. Thus, evidently, both NGC 6894 and NGC 6804 lie close to, but just below, the $\log n_e$ X-ray detection threshold. It is important to keep in mind that electron density is not a good indicator of PN evolutionary state. Fast evolving stars reach low luminosities at relatively high nebular densities, but remain undetected in diffuse X-rays (Steffen et al. 2008). Upper limit estimates and observations of additional nebulae similar to these—with $n_e \gtrsim$

1000 cm^{-3} and closed optical morphologies (multiple shells, well-defined inner bubbles)—will allow us to answer questions about diffuse emission such as the following. What is the lifetime of the hot bubble shaping phase? How does it relate to the mass of the CSPN progenitor? What is the relationship between diffuse X-ray emission and the final mass of the core, i.e., the WD remnant? We aim to revisit the question of diffuse X-ray dependence on age in R. Montez et al. (2014, in preparation; also see Schönberner et al. 2014).

4.3. Binary Detections/Non-detections

Six additional known binary CSPNe were observed in Cycle 14, all of which are close binaries ($p < 3$ days). Two of these six, NGC 6337 and Sp 1, had detectable point source X-ray emission. Both PNe appear to have nearly pole-on hourglass structures. The median energy for both point sources is relatively hard ($\gtrsim 1.0$ keV), which implies that the CSPN X-ray emission is due to late-type companions that display elevated levels of coronal activity. These binary, X-ray-luminous CSPN are therefore similar to the CSPNe in DS 1, HFG 1, and LoTr 5, which are thought to be systems in which mass transfer from PN progenitor to late-type companion has spun up the companion (Jeffries & Stevens 1996; Soker & Kastner 2002; Montez et al. 2010); alternatively, in many or most of these cases of X-ray-emitting binary CSPNe, it is possible the coronal activity of the companion is due to tidal locking that has resulted in rapid, synchronous rotation (a possibility we further explore in Montez et al. 2014). Both NGC 6337 and Sp 1 represent the two most compact (and therefore youngest) PNe harboring X-ray point sources at known binary CSPNe in the CHANPLANS sample (Figure 4). The periods of the close binaries within A65 (1.00 day; Bond & Livio 1990; Shimansky et al. 2009; T. Hillwig et al. 2014, in preparation), He 2-11 (0.61 days; Jones et al. 2014b), and NGC 6026 (0.53 days; Hillwig et al. 2010) lie between those of NGC 6337 (0.17 days; Hillwig et al. 2010) and Sp 1 (2.91 days; Bond & Livio 1990), but no point source X-ray emission was detected from the former three PNe. This leaves us with unanswered questions: What is the relationship between binary period/separation and X-ray point source emission? What are the characteristics of secondaries within binaries that do exhibit X-ray emission?

IC 5148/50 is a potentially significant non-detection, given its morphological similarity to Sp 1. Based on imagery alone, Sp 1 appears to have a spherical morphology, but spatiokinematical modeling reveals this is a projection effect and its intrinsic structure is that of a pole-on hourglass (Jones et al. 2012). Such bipolar structures are likely to be the products of binary interactions (see, e.g., Balick & Frank 2002, and references therein). The non-detection of IC 5148/50 may indicate that while it is morphologically similar to Sp 1, structurally it may be quite different. From Hα, [N II], and [O III] observations (Hua et al. 1998), it is clear that IC 5148/50 hosts not only internal elliptical structure but also a helical structure. Observations of H$_2$ (Kastner et al. 1996) and/or spatially resolved, high-resolution emission line spectroscopy (for use in spatiokinematical modeling) are necessary to determine whether or not IC 5148/50 has inherently bipolar versus elliptical structure. The CSPN of IC 5148/50 also has no infrared excess indicative of an unresolved cool companion (De Marco et al. 2013; Douchin et al. 2014).

It is possible that many other relatively X-ray-luminous CSPN have gone undetected in our sample of PNe. From Figure 5 we see that the fraction of PNe with detected point-like X-ray emission is strongly dependent on distance. All six sample PNe within $\lesssim 0.6$ kpc have point-like emission, whereas beyond 1.3 kpc the detection fraction drops to ~35%. This drop in detection fraction is likely the result of increased interstellar extinction obscuring the softer X-ray point sources, and furthermore implies that we lack the sensitivity necessary to detect even the (harder) binary CSPNe at distances much beyond ~1 kpc. Further discussion concerning the implications of the distance dependence of the X-ray detection rate of CSPNe can be found in Montez et al. (2014).

4.4. Diffuse X-Ray Emission from Jet–Wind Interactions During Common Envelope Ejection?

Several elliptical PNe display diffuse X-ray emission morphologies wherein the elongated diffuse emission appears to include peaks on two opposite locations along the long axis of the elliptical rim. Examples are NGC 3242, NGC 6543, NGC 7009, NGC 7662 (Paper I), and NGC 3918 (Figure 1). One possible interpretation of such an X-ray morphology, with far-reaching implications, is that the diffuse emission emanates from gas heated by shocks as low-mass jets with velocities of a few 100 km s^{-1} passed through material previously ejected in a common envelope interaction (Akashi et al. 2008). Such post-common envelope jets would most likely be launched by an accretion disk around a main sequence companion to the PN progenitor star during the progenitor's post-AGB phase. Indeed, it is possible that such jets are the "last gasps" of outflows launched during the final stages of common envelope evolution (Tocknell et al. 2014). If so, then the diffuse X-ray emission from elliptical PNe might hint at the operation of jets in the final removal of common envelopes formed by evolved, close binary systems. The X-ray emission morphologies of elliptical PNe, and their potential implications for common envelope models of PN formation, will be further explored in subsequence papers in the CHANPLANS series (e.g., R. Montez et al. 2014, in preparation).

5. SUMMARY

We present results from the most recent set of observations obtained by the *Chandra* Planetary Nebula Survey (CHANPLANS), the first comprehensive X-ray survey of PNe in the solar neighborhood (within ~1.5 kpc). The survey is designed to place constraints on the frequency of the appearance and range of X-ray spectral characteristics of X-ray-emitting PN central stars and the evolutionary timescales of wind-shock-heated bubbles within PNe. CHANPLANS began with a combined Cycle 12 and archive *Chandra* survey of 35 PNe. CHANPLANS continued via a *Chandra* Cycle 14 Large Program which targeted 24 additional compact ($R_{\rm neb} \lesssim 0.4$ pc), young PNe that lie within ~1.5 kpc. The highlights of the CHANPLANS Cycle 14 results include the following.

1. The overall X-ray detection rate for relatively compact ($\lesssim 0.4$ pc) PNe within ~1.5 kpc observed thus far by *Chandra* is ~54%.

2. Nearly 40% of the CHANPLANS sample PNe host X-ray-luminous point sources at their CSPNe. This includes three new detections of CSPNe X-ray sources within the Cycle 14 sample PNe.

3. Roughly 60% of the known binaries within the CHANPLANS sample display point-like X-ray emission, including first-time Cycle 14 detections of X-rays from the CSPNe of NGC 6337 and Sp 1.

4. All PNe with [WR]-type CSPN within the ChanPlaNS sample observed thus far (BD +30°3639, NGC 40, NGC 2371, NGC 1501, NGC 6369) display diffuse X-ray emission. With the exception of NGC 2371, all of these PNe have elliptical morphologies. In each case, the diffuse X-ray emission resembles the limb-brightened morphology of wind-blown bubbles blown by massive WR stars.

5. The addition of the Cycle 14 results brings the overall ChanPlaNS diffuse X-ray detection rate to ∼27%.

6. It has become clearer that diffuse X-ray emission is associated with young ($\lesssim 5 \times 10^3$ yr) PNe with compact ($R_{neb} \lesssim 0.15$ pc), closed structures and high central electron densities ($n_e \gtrsim 1000$ cm^{-3}). Typically, such nebulae display nested-shell elliptical morphologies and rarely show H_2 emission and/or pronounced butterfly structures. Hb 5 is a notable exception.

7. The ChanPlaNS detection rate of diffuse X-ray emission from PNe within ∼1.5 kpc appears largely independent of distance and excitation, if the latter is measured via the flux ratio of [O III] and Hβ lines.

8. In contrast, the ChanPlaNS detection rate of point-like X-ray emission from PNe within ∼1.5 kpc appears strongly dependent on distance, reflecting the relatively low intrinsic X-ray luminosities of CSPNe combined with the effects of interstellar extinction.

We note that in addition to the need to acquire data for a larger sample of PNe—particularly high-n_e PNe and those harboring known binary central stars—we must carry out estimations of upper limits on L_X in order to reaffirm our claims and to properly answer our open questions. Further analysis of these and future ChanPlaNS data and results describing both point-like X-ray emission from CSPNe (Montez et al. 2014) and diffuse X-ray emission from PNe (R. Montez et al. 2014, in preparation) will continue to refine models of PN shaping mechanisms, X-ray emission timescales, and the role of binarity in PN formation and evolution.

REFERENCES

Akashi, M., Meiron, Y., & Soker, N. 2008, NewA, 13, 563
Bagnulo, S., Landstreet, J. D., Fossati, L., & Kochukhov, O. 2012, A&A, 538, 22
Balick, B., & Frank, A. 2002, ARA&A, 40, 439
Bernard-Salas, J., & Tielens, A. G. G. M. 2005, A&A, 431, 523
Bilíková, J., Chu, Y.-H., Gruendl, R. A., & Maddox, L. A. 2010, AJ, 140, 1433
Bilíková, J., Chu, Y.-H., Gruendl, R. A., Su, K. Y. L., & De Marco, O. 2012, ApJS, 200, 3
Bodman, E. H. L., Schaub, S. C., & Hillwig, T. 2012, JSARA, 5, 19
Boffin, H. M. J., Miszalski, B., Rauch, T., et al. 2012, Sci, 338, 773
Bohigas, J. 2001, RMxAA, 37, 237
Bond, H. E., & Livio, M. 1990, ApJ, 355, 568
Cassinelli, J. P., Cohen, D. H., Macfarlane, J. J., Sanders, W. T., & Welsh, B. Y. 1994, ApJ, 421, 705
Clegg, R. E. S., Harrington, J. P., Barlow, M. J., & Walsh, J. R. 1987, ApJ, 314, 551
Corradi, R. L. M., Perinotto, M., Villaver, E., Mampaso, A., & Gonçalves, D. R. 1999, ApJ, 523, 721
Corradi, R. L. M., Sabin, L., Miszalski, B., et al. 2011, MNRAS, 410, 1349
Crowther, P. A., De Marco, O., & Barlow, M. J. 1998, MNRAS, 296, 367
Crowther, P. A., Morris, P. W., & Smith, J. D. 2006, ApJ, 636, 1033
De Marco, O. 2009, PASP, 121, 316
De Marco, O., Passy, J.-C., Frew, D. J., Moe, M., & Jacoby, G. H. 2013, MNRAS, 428, 2118
De Marco, O., Passy, J. C., Moe, M., et al. 2011, MNRAS, 411, 2277
DePew, K., Parker, Q. A., Miszalski, B., et al. 2011, MNRAS, 414, 2812
Douchin, D., De Marco, O., Frew, D. J., et al. 2014, MNRAS, submitted
Drew, J. E., Gonzalez-Solares, E., Greimel, R., et al. 2014, MNRAS, 440, 2036
Dwarkadas, V. V., & Rosenberg, D. L. 2013, HEDP, 9, 226
Ercolano, B., Morisset, C., Barlow, M. J., Storey, P. J., & Liu, X. W. 2003, MNRAS, 340, 1153
Ercolano, B., Wesson, R., Zhang, Y., et al. 2004, MNRAS, 354, 558
Frew, D. J. 2008, PhD thesis, Macquarie Univ.
Frew, D. J., Bojičić, I. S., Parker, Q. A., et al. 2014a, MNRAS, 440, 1080
Frew, D. J., Parker, Q. A., & Bojičić, I. S. 2014b, MNRAS, submitted
Freyer, T., Hensler, G., & Yorke, H. W. 2003, ApJ, 594, 888
García-Díaz, M. T., Clark, D. M., López, J. A., Steffen, W., & Richer, M. G. 2009, ApJ, 699, 1633
García-Segura, G., Langer, N., & Mac Low, M. M. 1996a, A&A, 316, 133
García-Segura, G., Mac Low, M. M., & Langer, N. 1996b, A&A, 305, 229
Guerrero, M. A., & De Marco, O. 2013, A&A, 553, A126
Guerrero, M. A., Toalá, J. A., Medina, J. J., et al. 2013, A&A, 557, A121
Herald, J. E., & Bianchi, L. 2011, MNRAS, 417, 2440
Hillwig, T. C., Bond, H. E., Afşar, M., & De Marco, O. 2010, AJ, 140, 319
Hillwig, T. C., Frew, D. J., Louie, M., et al. 2014, AJ, submitted
Hua, C. T., Dopita, M. A., & Martinis, J. 1998, A&AS, 133, 361
Huckvale, L., Prouse, B., Jones, D., et al. 2013, MNRAS, 434, 1505
Jacob, R., Schönberner, D., & Steffen, M. 2013, A&A, 558, A78
Jeffries, R. D., & Stevens, I. R. 1996, MNRAS, 279, 180
Jones, D., Boffin, H. M. J., Miszalski, B., et al. 2014a, A&A, 562, A89
Jones, D., Mitchell, D. L., Lloyd, M., et al. 2012, MNRAS, 420, 2271
Jones, D., Santander-Garcia, M., Boffin, H. M. J., Miszalski, B., & Corradi, R. L. M. 2014b, in Asymmetrical Planetary Nebulae VI conference, ed. C. Morisset, S. Delgado Inglada, & S. Torres Peimbert, http://www.astroscu.unam.mx/apn6/PROCEEDINGS/ (arXiv:1401.4119)
Jordan, S., Bagnulo, S., Werner, K., & O'Toole, S. J. 2012, A&A, 542, A64
Jordan, S., Werner, K., & O'Toole, S. J. 2005, A&A, 432, 273
Kastner, J. H., Montez, R., Jr., Balick, B., & De Marco, O. 2008, ApJ, 672, 957
Kastner, J. H., Montez, R., Jr., Balick, B., et al. 2012, AJ, 144, 58
Kastner, J. H., Weintraub, D. A., Gately, I., Merrill, K. M., & Probst, R. G. 1996, ApJ, 462, 777
Kwok, S., Purton, C. R., & Fitzgerald, P. M. 1978, ApJL, 219, L125
Leone, F., Martínez González, M. J., Corradi, R. L. M., Privitera, G., & Manso Sainz, R. 2011, ApJL, 731, L33
Li, J., Kastner, J. H., Prigozhin, G. Y., et al. 2004, ApJ, 610, 1204
López, J. A., García-Díaz, M. T., Steffen, M., Riesgo, H., & Richer, M. G. 2012, ApJ, 750, 131
Marten, H., & Schönberner, D. 1991, A&A, 248, 590
Miszalski, B., Corradi, R. L. M., Boffin, H. M. J., et al. 2011, MNRAS, 413, 1264
Monteiro, H., Schwarz, H. E., Gruenwald, R., & Heathcote, S. 2004, ApJ, 609, 194
Montez, R., Jr., De Marco, O., Kastner, J. H., & Chu, Y.-H. 2010, ApJ, 721, 1820
Montez, R., Jr., & Kastner, J. H. 2013, ApJ, 766, 26
Montez, R., Jr., Kastner, J. H., Balick, B., et al. 2014, ApJ, submitted
Montez, R., Jr., Kastner, J. H., Balick, B., & Frank, A. 2009, ApJ, 694, 1481
Montez, R., Jr., Kastner, J. H., De Marco, O., & Soker, N. 2005, ApJ, 635, 381
Nordhaus, J., Blackman, E. G., & Frank, A. 2007, MNRAS, 376, 599
Parker, Q. A., Phillipps, S., Pierce, M. J., et al. 2005, MNRAS, 362, 689
Patriarchi, P., & Perinotto, M. 1991, A&A, 91, 325
Peña, M., Rechy-García, J. S., & García-Rojas, J. 2013, RMxAA, 49, 87
Perinotto, M., Schönberner, D., Steffen, M., & Calonaci, C. 2004, A&A, 414, 993
Pottasch, S. R., & Bernard-Salas, J. 2010, A&A, 517, A95
Ramos-Larios, G., Guerrero, M. A., Vazquez, R., & Phillips, J. P. 2012, MNRAS, 420, 1977
Ramos-Larios, G., Guerrero, M. A., Vazquez, R., & Phillips, J. P. 2013, arXiv:1305.4211
Sahai, R., Morris, M. R., & Villar, G. G. 2011, AJ, 141, 134
Schmidt-Voigt, M., & Koppen, J. 1987, A&A, 174, 223

Schönberner, D., Jacob, R., Lehmann, H., et al. 2014, AN, 335, 378
Shimansky, V. V., Pozdnyakova, S. A., Borisov, N. V., et al. 2009, AstBu, 64, 349
Soker, N., & Kastner, J. H. 2002, ApJ, 570, 245
Soker, N., & Livio, M. 1994, ApJ, 421, 219
Soker, N., & Rappaport, S. 2000, ApJ, 538, 241
Steffen, M., Schönberner, D., & Warmuth, A. 2008, A&A, 489, 173
Su, K. Y. L., Chu, Y.-H., Rieke, G. H., et al. 2007, ApJL, 657, L41

Toalá, J. A., & Arthur, S. J. 2011, ApJ, 737, 100
Toalá, J. A., & Arthur, S. J. 2014, MNRAS, 443, 3486
Toalá, J. A., Guerrero, M. A., Chu, Y.-H., et al. 2012, ApJ, 755, 77
Tocknell, J., De Marco, O., & Wardle, M. 2014, MNRAS, 439, 2014
Vázquez, R., Miranda, L. F., Torrelles, J. M., et al. 2002, ApJ, 576, 860
Villaver, E., Manchado, A., & García-Segura, G. 2002, ApJ, 581, 1204
Webster, B. L., Payne, P. W., Storey, J. W. V., & Dopita, M. A. 1988, MNRAS, 235, 533